Can. Aeronaut. Space J., Vol. 59, No. 2, pp. 1–11, 2013

Design of a lunar dust resistant connection interface using biomimetic strategies

Vincent Biron, Mathieu Lalumière Boucher, Alaric Bergeron, Frédérick Marcil-St-Onge, Nima Gharib, Jacques Luk-Cyr, Marie-Josée Potvin, Li Shu, and Peter Radziszewski

Abstract. In lunar exploration, dust poses a significant problem due to its pervasiveness, adherence, and abrasiveness, causing premature failure of mechanisms. Successful operation of autonomous equipment in the harsh lunar environment requires innovative methods of dust protection, especially for exposed connection interfaces. In eventual robotic lunar exploration missions, lunar dust control will be a major factor affecting mission lifetimes and operations. Biomimetic inspired concepts are developed to design an interface allowing electrical connection between a lunar rover and interchangeable instruments. A proof-of-concept prototype of the interface has been constructed to demonstrate system functionality under laboratory conditions.

Résumé. Dans le cadre de l'exploration lunaire, la poussière représente une difficulté importante à cause de son omniprésence, de son adhérence et de sa capacité d'abrasion, tout ceci menant à des bris prématurés des mécanismes. Des méthodes innovantes en protection contre la poussière sont requises pour réussir à faire fonctionner de l'équipement de façon autonome, particulièrement en ce qui concerne les interfaces de connexion exposées à l'environnement. Lors d'éventuelles missions lunaires robotiques, le contrôle de la poussière lunaire sera un facteur déterminant pour la durée de la mission et pour le type d'opérations possibles. Des concepts inspirés de la biomimétique sont développés pour concevoir une interface permettant une connexion électrique entre une plateforme mobile lunaire et des instruments interchangeables. Un prototype de l'interface est construit pour démontrer la fonctionnalité du système dans des conditions de laboratoire.

List of symbols

a	area
$\vec{B}$	magnetic force
e	coefficient of restitution
$\vec{F}_L$	Lorenz force
F_n	normal force
$\vec{F}_P$	paramagnetic force
F_t	tangential force
G	equivalent shear modulus
I	current
K_B	Boltzmann's constant
m	equivalent mass
$\vec{m}$	magnetic moment
$\vec{M}$	induced magnetic moment
N	number of coils
q	charge of a particle
r	radius
R	equivalent radius
R_i	distance between of contact point to the center of mass of the object
$\vec{S}$	velocity
S_n	normal stiffness
S_t	tangential stiffness
T	temperature
U	electrostatic potential
V_n^{rel}	normal component of the relative velocity
V_t^{rel}	tangential component of the relative velocity
Y	equivalent Young's modulus
β	normal stiffness
δn	normal overlap
δt	tangential overlap
ε	relative permittivity
λ	Debye length
τ_i	torque at the contact point
μ_0	magnetic permeability
μ_r	coefficient of rolling friction
ω_i	unit angular velocity of the object at the contact point
χ_m	magnetic susceptibility

Received 28 September 2010. Accepted 31 January 2013. Published on the Web at http://pubs.casi.ca/journal/casj on 7 June 2013.

Vincent Biron,[1] Mathieu Lalumière Boucher, Alaric Bergeron, Frédérick Marcil-St-Onge, Jacques Luk-Cyr. École Polytechnique de Montréal, 2900 Boulevard Edouard-Montpetit, Montréal, QC H3T 1J4.

Nima Gharib and Peter Radziszewski. McGill University, 845 Sherbrook Street West, Montréal, QC H3A 0G4.

Marie-Josée Potvin. Canadian Space Agency, 6767 Route de l'Aéroport Saint-Hubert, QC J3Y 8Y9.

Li Shu. University of Toronto, 563 Spadina Crescent, Toronto, ON M5S 2J7.

[1]Corresponding author (e-mail: houlabaga@hotmail.com).

Vol. 59, No. 2, August/août 2013

Introduction

At the onset of the Apollo missions, little was known about lunar dust. Mechanisms were built according to standards used for dusty environments on earth. However, lunar dust is comprised of highly abrasive, electrically charged particles with sizes ranging from 1/100th of a micron to 100 microns. The electrostatic properties come from the small amount of iron present in the dust, allowing it also to react to magnetic fields.

During the Apollo missions, dust posed a significant problem due to its pervasiveness, adherence, and abrasiveness, causing premature failure of structures and mechanisms. Solar winds charge the dust particles, and as a result, these particles float above the surface for extended periods of time. Any motion at the surface displaces the dust, and the combined effect of low gravity and electrostatic properties sends the dust in the air at a certain speed.

Future lunar missions will involve rovers that can stay on the moon for extended periods of time to collect the maximum amount of scientific data, and potentially, the capacity to switch payloads. Switching payloads on a rover will require a connecting interface. The pervasive lunar dust could hamper this capacity. As dust clings to all surfaces, any connecting interface needs to be cleaned of its dust prior to connection or to be sealed until the connection occurs. The goal of this project was to design a connecting interface for the lunar environment. Biomimetic methods were used to generate ideas.

Lunar dust

Lunar regolith adheres strongly to all surfaces. The mechanical aspect of adhesion is due to the jagged shape of regolith particles as shown in **Figure 1**. The absence of an atmosphere means there is no wind that would otherwise round regolith particles, resulting in sharp edges (Stubbs et al., 2005). While **Figure 2** shows a fairly large particle, most particles are below 70 μm in diameter; therefore, they are very fine grained and will even abrade mechanical seals (Zakrajsek et al., 2005).

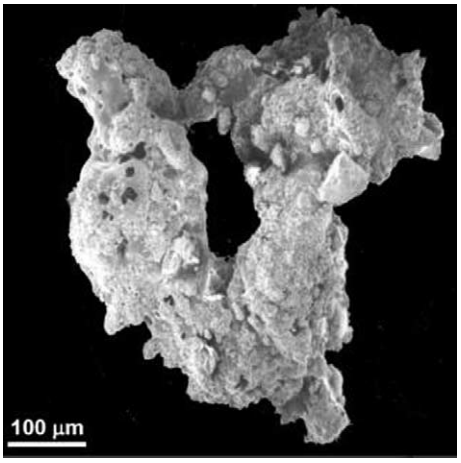

Figure 1. Lunar regolith particle. Image Credit: David S. McKay, NASA/JSC, permission granted.

Regolith contains a small fraction of iron. The particles get charged by solar wind in the day and plasma electron currents at night, and this leads to electrostatic adhesion (Stubbs et al., 2005). This electrostatic charging enables particles to cling to ungrounded conductive surfaces and nonconductive surfaces. The solar wind charges the particles positively during the daytime, and the electron plasma currents charge the particles negatively at night. Finer regolith grains will levitate under electrostatic charging and, therefore, the dust is present at instrument level, even in the absence of any mechanical disturbance of the soil. This makes the dust highly pervasive, even a few metres above the ground. It is this pervasiveness that leads to the need of a specific design for any connector used on the moon.

Biomimetic design

In biomimetic design, biological phenomena serve as stimuli for solving engineering problems. An often-cited example of biomimetic design is how Velcro emulates the hook structures found on burrs that were observed to attach

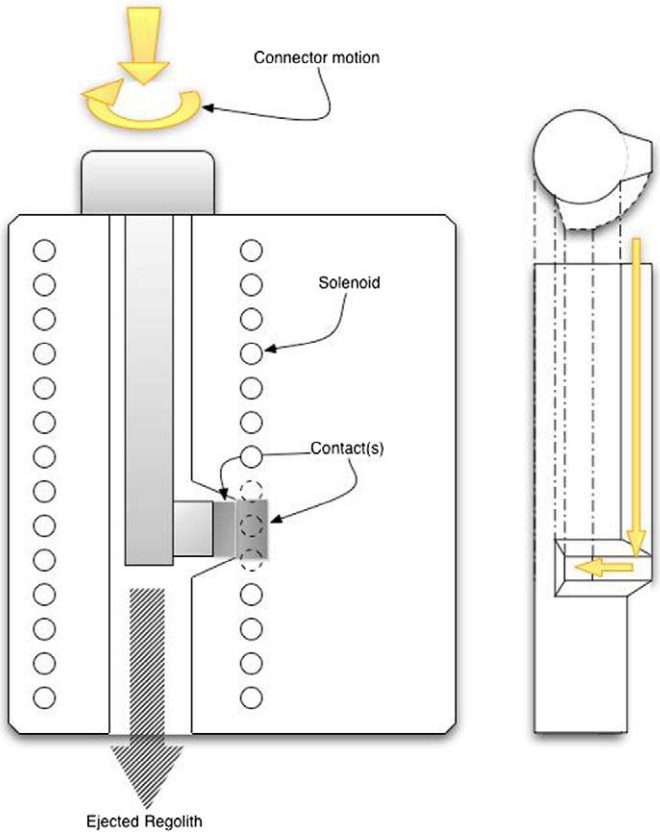

Figure 2. "Twist and lock" connector design.

to fur and clothing. While Velcro resulted from the designer's own experience with burrs, many designers may not know of all the relevant biological phenomena that could solve a given problem. Also, the creation of a database to catalog all of the biological phenomena for engineering design is a formidable task that is also subject to the compilers' personal bias. Therefore, Vakili and Shu (2001) developed a method to search existing biological knowledge in natural-language format to identify relevant biological analogies. The initial corpus, or text, is an undergraduate level biology textbook, *Life, the Science of Biology* (2001). Search keywords correspond to verbs that describe the desired function of the solution, and identify biological phenomena that can be used either directly for a design solution or as a starting point for further research into useful biological phenomena.

Because we were seeking design solutions that "protect" equipment from lunar regolith, an obvious starting keyword that describes the intended function of our solution was protect. Because we were searching for instances of keywords in natural language as opposed to a database using specified keywords, a first step was to find synonyms or other words related to the initial keywords. For example, "defend" is a keyword related to protect. Chiu and Shu (2007) found that because of lexical differences between biology and engineering domains, searching biological knowledge in natural-language format for instances of engineering keywords may not yield good results. Therefore a method was developed that identifies biologically meaningful keywords. This method uses a combination of word collocation (which words occur together in an excerpt) and frequency analysis (how frequently words occur in an excerpt). Chiu and Shu (2007) confirmed that the keyword defend is related to "remove", in that biological entities "remove/clean" themselves as a defensive mechanism. Furthermore, troponyms (or more specific manners) of remove include "pull", "harvest", "eliminate", "excrete", "shed", "draw", "pump", and "kill".

Searching for instances of excrete revealed how most animals have tubular guts that excrete waste. Furthermore, peristalsis is a wave of smooth muscle contraction that moves food through the gut. How peristalsis moves food through the gut is used as an analogy for how to move lunar regolith.

Concept

As stated in the previous section, the prototype design was based on peristalsis. The concept focused on a tubular connection interface surrounded by magnetic coils as shown in **Figure 2**. These coils are driven by synchronized currents to induce varying magnetic gradients through the tunnel. The lunar regolith particles, being ferromagnetic, will react to the magnetic gradients, and a force proportional to the square of the field gradient will be exerted on them, thus expelling them from the connection tube. The connecting area can therefore be cleaned of its dust prior to connection. Because there are no moving mechanical parts to protect the connecting area, the risks of degradation due to dust or failure are minimized.

The connector itself was based on a "twist and lock" mechanism, allowing for easy manipulation by astronauts while ensuring a reliable and secure connection. The male connector has a right-angled head, which fits in a side groove in the connector body.

Before the connection is made, the connector body goes through an ejection cycle. During this cycle, a high current pulse is sent to the coil, generating a high magnetic gradient inside the connector, thus ejecting the dust present in it. The grooves in the connector body are all tapered to avoid dust buildup and allow easy flowing of the dust during its ejection. In the event that the male connector is covered in dust, another ejection cycle can be executed with the connector head inserted to remove the regolith. Once the connector head is fully inserted and free of dust, a quarter-turn rotation secures it in place and brings the conductive plates of the connector head and body in contact with each other, completing the connection maneuver.

To obtain a satisfactory gradient distribution ensuring a directional particle flow along the axis of the connector, it was determined that the coils surrounding the tube had to be wound in such a way that each coil overlaps half of the preceding and following coil, as shown in **Figure 3**. This design optimizes gradient distribution in the tube, as the gradient of the field generated by a current coil is maximal at its extremities and nearly nil at the center. By winding the coils in this fashion, we guaranteed that every region of the tube where field gradient is low when one set of coils is enabled will present a maximal gradient when other coils are activated. This will have the effect of eliminating any stale regions in the tube where the dust would never be exposed to high gradients. By activating the coils sequentially, we effectively carried the dust along the tube by creating zones of high gradient one in front of another along the length of the tube. The first prototype was designed as a horizontal tube, with seven overlapping wire coils around it as shown in

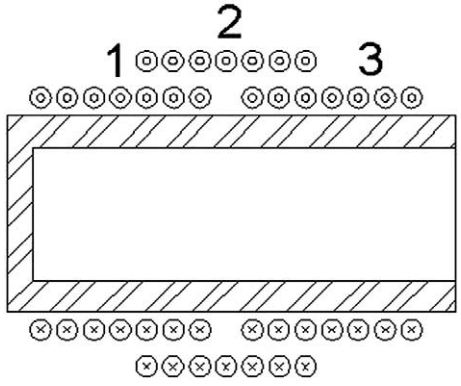

Figure 3. Sectional view of the tube and coils.

Vol. 59, No. 2, August/août 2013

Figure 3. The tube was made of aluminum, a nonferromagnetic metal, to maximize magnetic field penetration inside the tube. The coils were hand-wound at about 600 turns each using standard 29 AWG (American wire gauge) coated copper winding wire. The tube itself has an external diameter of 19 mm and a length of 10.16 cm, each of the coils spanning about 2.54 cm along the tube.

Physical model

Paramagnetic particles (such as iron-rich lunar regolith) are subjected to a net force when placed in a nonuniform magnetic field or a magnetic field gradient. Such a field can be obtained by circulating current around a conductive loop.

In the case of a long solenoid (wire coil), the magnetic field can be considered uniform at the center of the coil, and as such the gradients and paramagnetic forces are weak. However, the field diverges at the extremities of such a coil and thus there are elevated gradients at these extremities, as represented in **Figure 4**. Such a divergence is called the "edge effect" and is of primary importance in this design, as it provides the driving force to move the regolith particles.

To maximize this edge effect, we used short coils so that the uniform-field section was reduced to a minimum. Furthermore, to ensure that the particles were constantly surrounded by a high field gradient, several coils overlapped each other so that the lowest field gradient section of one coil was coincident to the highest field gradient of the next. These coils were then activated sequentially to generate a kind of magnetic peristaltism, causing the particles to migrate from one coil to the next.

Concurrent to this paramagnetic effect, the regolith particles, which possess an electrostatic charge, should also be submitted to a Lorentz force. This force describes the behaviour of a particle of charge q moving at speed $\vec{s}$ in a magnetic field of strength $\vec{B}$. The resulting force is given as $\vec{F}_L = q(s \times \vec{B})$. As this force is the result of a vector product between the speed of the particle and the magnetic field, it is perpendicular to both these vector quantities and as such was of very little interest to us. Indeed, we sought to accelerate the particles linearly and a perpendicular acceleration only induced a circular (or helicoidal) motion. However, our experiments to date have not induced a very high speed in the particles, and consequently, we neglected this Lorentz force in this mathematical treatment.

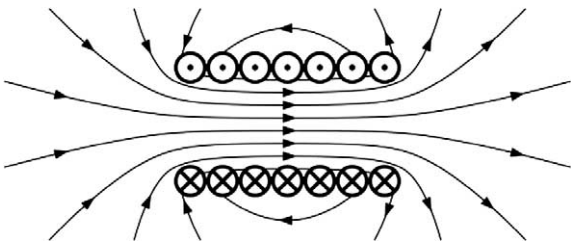

Figure 4. Magnetic field lines inside a current coil.

The paramagnetic force exerted on a ferromagnetic particle of magnetic susceptibility χ_m placed in a magnetic field B_0 is given by

$$\vec{F}_p = \nabla(\vec{M} \bullet \vec{B}_0) \tag{1}$$

where $\vec{M} = \frac{\chi_m \vec{B}}{\mu_0}$ is the induced magnetic moment, in the particle, thus giving

$$\vec{F}_p = \frac{\chi_m}{\mu_0} \nabla \left|\vec{B}_0\right|^2 \tag{2}$$

If we consider N coils of current I and of area a, the field $\vec{B}_0$ they produce is equivalent to the one produced by a magnetic moment $\vec{m} = NIa\hat{m}$, which can be expressed as

$$\vec{B}_0(\vec{r}) = \frac{\mu_0}{4\pi} \frac{3\vec{r}(\vec{m} \bullet \vec{r}) - \vec{m}r^2}{r^5} \tag{3}$$

For a coil along the z axis, $\vec{m} = (0, 0, NIa)$ and

$$\begin{aligned} \left|\vec{B}_0(\vec{r})\right|^2 &= \left|\frac{\mu_0}{4\pi} \frac{3\vec{r}((0,0,NIa) \bullet \vec{r}) - (0,0,NIa)r^2}{r^5}\right|^2 \\ &= \left(\frac{3\mu_0 NIa}{4\pi} \frac{xy}{r^5}\right)^2 \end{aligned} \tag{4}$$

Thus, the force is given by

$$\vec{F}_P = \frac{\chi_m}{\mu_0} \nabla \left|\vec{B}_0\right|^2 = \frac{\chi_m}{\mu_0} \nabla \left(\frac{3\mu_0 NIa}{4\pi} \frac{xy}{r^5}\right)^2 \tag{5}$$

The complete expression of this force is too large and unpractical to justify its presentation here, but it can be easily be obtained from Equation (5) by computing the value of the gradient. However, we can rather simply obtain a numerical approximation of the value of this gradient.

Considering coils formed by $N = 50$ loops of current of radius $r = 3/8$, the regolith particles are composed of approximately 2% iron (Stubbs et al., 2005). We approximated their apparent magnetic susceptibility as a linear combination of the susceptibility of its components. Supposing that the iron content of the regolith was in the form of iron oxides and that other components of the lunar dust were nonmagnetic, we obtained

$$\chi_m \approx 0,02\chi_m^{FeO} = 0,02 \times 720 \times 10^{-5} = 14,4 \times 10^{-5} \tag{6}$$

To get an idea of the gradient surrounding the extremity of such a coil, we defined a hemispheric surface S of radius r centred on the coil, as represented in **Figure 5**:

By integrating the gradient of the squared field intensity over the surface S, we obtained an approximation of the value of the field gradient in the vicinity of the coil

$$\left\rangle \nabla \left|\vec{B}_0\right|^2 \right\langle_S = \frac{\iint_S \nabla \left|\vec{B}_0\right|^2 \mathrm{d}\vec{A}}{\iint_S \mathrm{d}\vec{A}} \tag{7}$$

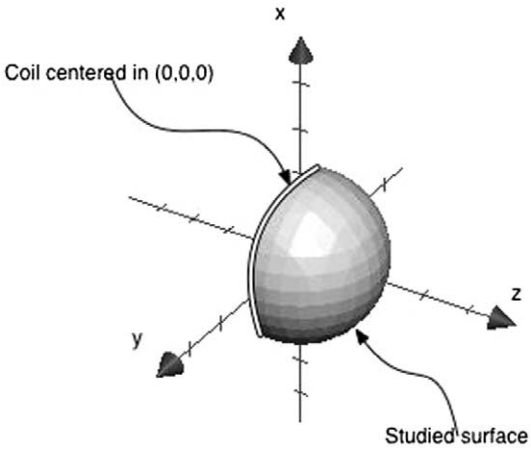

Figure 5. Definition of surface *S*.

A computer numerical calculation gave a value of

$$\left\langle \nabla \left| \vec{B}_0 \right|^2 \right\rangle_S \approx 9,6 \times 10^{-10} \frac{\mu_0^2 N^2 I^2}{\pi \sqrt{a}} \tag{8}$$

With the previously defined parameters and a current of 1 amp we obtained an average force of

$$\left\langle \vec{F}_P \right\rangle_S \approx 1,64 \times 10^{-14} N \tag{9}$$

over the whole surface. This rather small value prompted us to investigate different means of increasing the field gradient. Increasing the current and number of coils showed the most promise given their squared influence on the resulting force. Further experimental testing is needed to determine feasibility.

Electrical design

In the first version of the circuit, the current was supplied to the coils by a standard 12 V DC power supply with a current limiter. The coils were supplied with 3 amps of current which was later found to be insufficient to achieve the desired results. To achieve the coil lightning sequence, RKA-7D-12 relays were used. They also provided electrical isolation between the coils and the electronic control circuit, which can be easily damaged by inductive charges powering on and off. The enabling sequence signal was provided by a general purpose PIC16F690 8-bitCMOS microcontroller. It was used in output mode and provided seven different digital signals. The relays needed 12 V and 261 mW to switch into the "on" position. Being unable to supply such current and voltage, two standard L293D push–pull four-channel drivers with diodes were used. They provided the voltage and current required by the relays, and they also isolated the microcontroller from the switching coils activating the relays' switches. Power was supplied to the electronic control circuit with two standard 9 V batteries providing 18 V. This voltage was lowered to 5 V for the microcontroller and 12 V for the push–pull chips using standard LM7805 and LM7812 tension regulators. This is schematized in **Figure 6**.

In the second version of the circuit, schematized in **Figure 7**, a higher current running through the coils was needed. Changes were made from the first circuit to satisfy that criteria. The power supply for the coils was the main change between the two circuits. To achieve a larger instantaneous current, each coil was connected by its relay to a 470 μF 350 V charged capacitor. The capacitors were charged using a single 1.5 V AA battery. A step-up circuit raised the voltage to 350 V to allow the capacitors to be fully charged. The step-up circuits used were disposable camera flash capacitor charging circuits. They raised the voltage to the desired 350 V, were activated by a button, featured a status LED that lit up when the capacitor was fully charged, and they were commercially available. Another change that was made in the second version was the number coils went from 7 to 3.

The control circuit

The enabling sequence signal was provided by a general purpose PIC16F690 8-bit CMOS microcontroller. Pins were used as a basic I/O ports. Six of the pins were used as outputs for both sending the trigger signal to the relays and for the status LED. A single port was used as an input to read the trigger dip switch. When the microcontroller detected a rising front on the trigger switch, all relays were

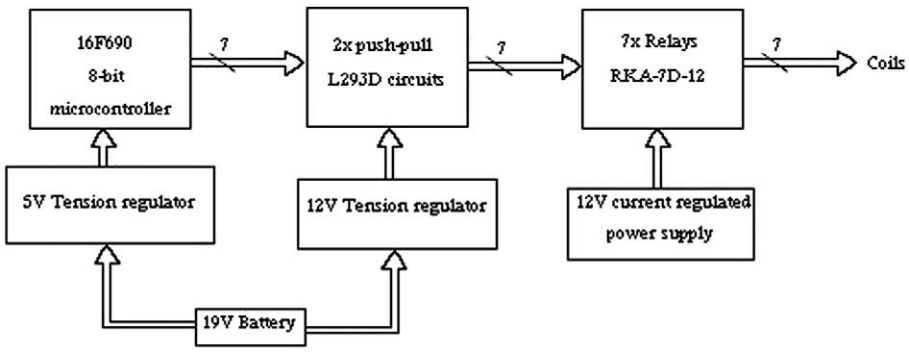

Figure 6. Schematized first version of the circuit.

Vol. 59, No. 2, August/août 2013

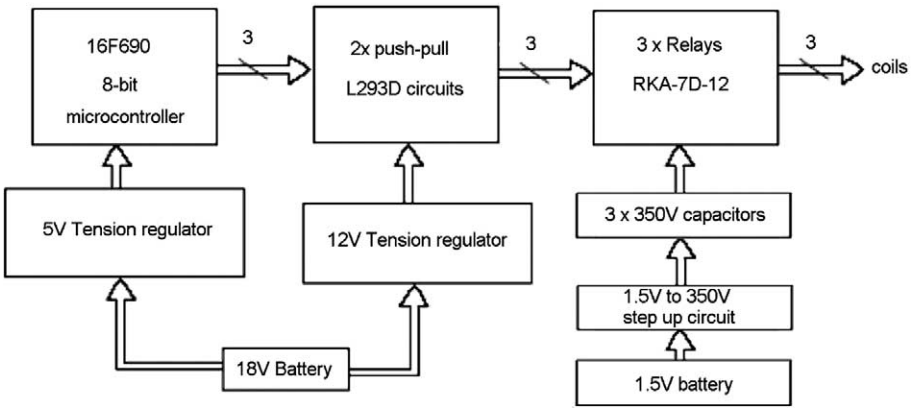

Figure 7. Schematized second version of the circuit.

returned to their open position and a white LED lit up. Then, the program would be in a waiting loop indicated by a single green illuminated LED. At this point, the control circuit was in a stable armed position and the capacitors could safely be charged. When the orange light on each step-up circuit lit up, indicating the capacitors were charged, the circuit was ready to be activated. Upon the activation of the circuit (trigger switch on the low 0 V position), the coil activation sequence would take place and the control circuit would return to the initial unarmed sequence.

General overview of the circuit

Figure 8 shows the circuit as seen from above; different parts are highlighted on the picture. The green rectangle shows the control circuit that activates the coils with the relays. The red rectangle shows the coils in which the dust is inserted. The yellow border shows the capacitor charge circuit. Once charged, the capacitors are connected to the coils by the relays activated by the charge circuit. The blue rectangle is the 18 V battery used by the control circuit and the 1.5 V cell used to charge the capacitors. The black border shows the controlled area on which the dust is expelled in the experiment.

The activation sequence

The coils were activated in the order marked on the tube on **Figure 3**. The sequence is described as Coil 1, wait 1 s, Coil 2, wait 0.3 s, and Coil 3. The coils were left activated for

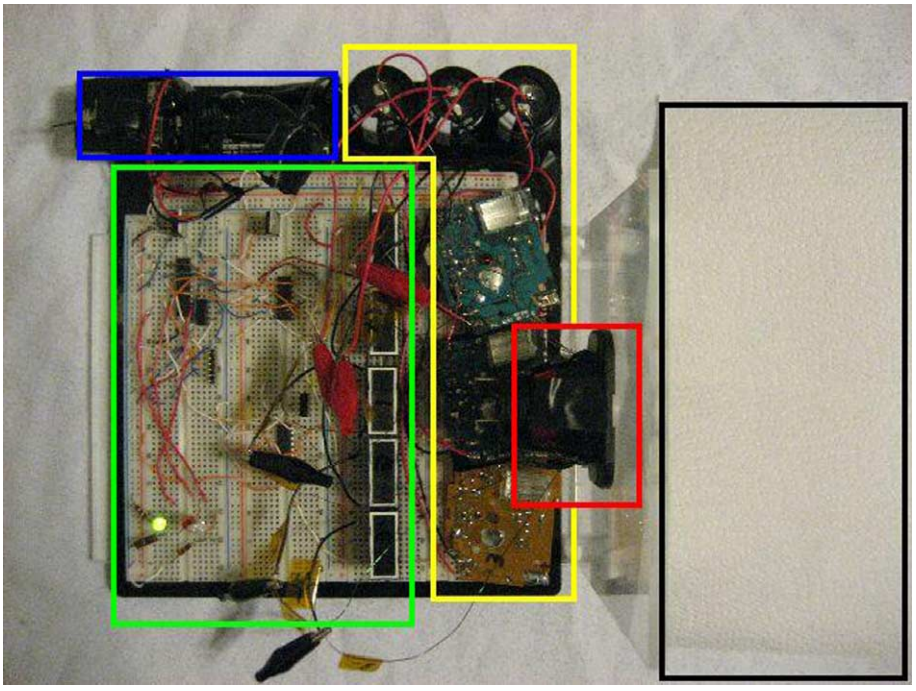

Figure 8. Circuit overview.

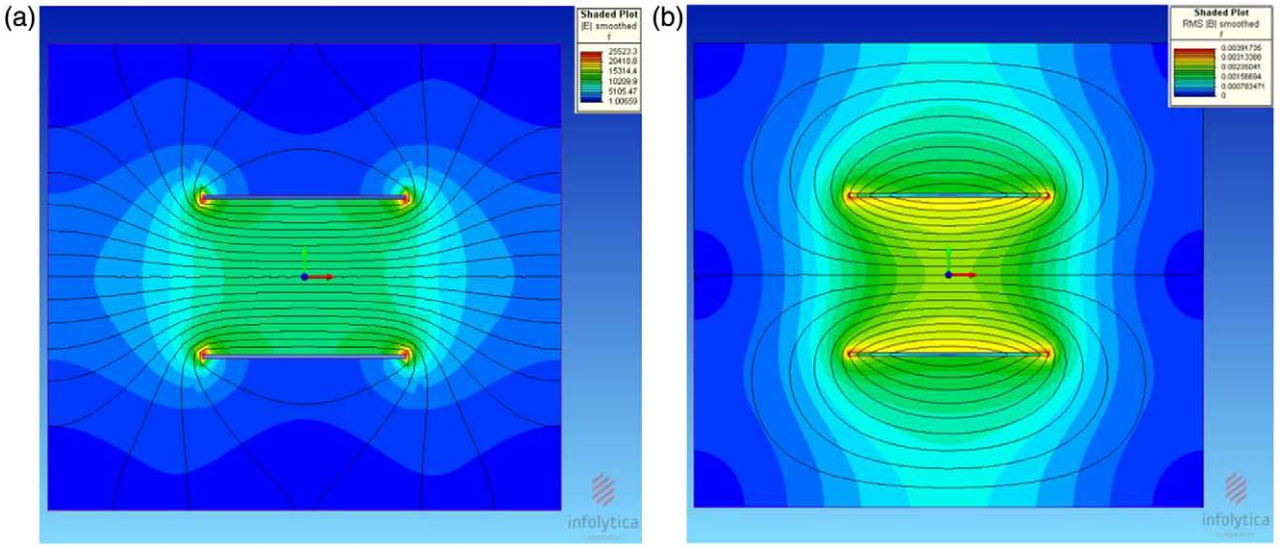

Figure 9. Finite element modeling of (a) electric field and (b) magnetic field generated by one coil.

a few seconds and then return to the inactivated position. The voltage supplied to the coils was not forced by the control circuit. Upon activation of the relays, the capacitors and coils circuit was left to discharge according to the system dynamic.

Simulation

Simulating the dust motion within the coil is highly interesting to evaluate the force of the field necessary to expel the dust and to extend results obtained on Earth to results expected on the moon. In the first part of the simulation, the electric and magnetic fields generated by the three coils were determined using MagNet and ElecNet software. The resulting fields then were imported to a discrete element modelling (DEM) software that uses the discrete element method to model particle movements.

Finite element modeling

MagNet and ElecNet are two packages developed by Infolytica Corporation. They use the finite element method (FEM) to model and predict the performance and behavior of any electrical devices. We modeled the electric field and magnetic field of one coil with the same dimension used in the experiment. The coil was modeled as a thin layer of cylinder (thickness of 1 mm and 100 turns) enclosed in a larger cylinder. Copper properties were assigned for the coil and air was selected as the surrounding environment. The material was assumed to behave linearly. The field flux was assumed to be normal to the outer boundary. The domain was meshed with triangular elements using a fine mesh near the coil. The solution method was set as Newton–Raphson. The resulting fields are shown in **Figure 9** in a plane cut through the cylindrical geometry.

Discrete element modeling

The discrete element method was developed in the early 1970s and has been applied to a wide range of problems with particulate media such as soil and rock problems, solid–gas interactions, and solid–liquid interactions (Houge et al., 2008). With recent advances in computing technology, it can also be applied to the traditional continuum problems. In this work, a DEM software was used to simulate the particle movements under electrostatic and electromagnetic forces.

Three cylindrical geometries were created to model the overlapping coils. The material properties of the cylinders are listed in **Table 1**.

One hundred spherical particles were created along the cylinder with $r = 0.5$ mm and Std. Dev. $= 0.2$. The interaction between particles was governed by the contact model.

Contact model

The Hertz–Mindlin contact model was used to define the interaction between the particles (Houge et al., 2008). It can be schematized as the configuration shown in **Figure 10** where normal and tangential reactions are transmitted by corresponding parallel connected springs and dampers.

Table 1. Material properties.

Poissin's ratio	0.25
Shear modulus	1e08 *Pa*
Density	1000 kg/m^3
Work function	0.4 *eV*
Coefficient of restitution	0.5
Coefficient of static friction	0.5
Coefficient of rolling friction	0.01

Vol. 59, No. 2, August/août 2013

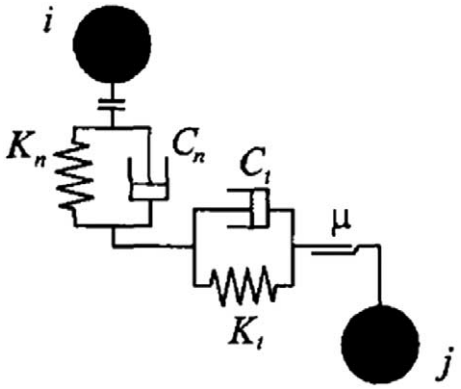

Figure 10. DEM contact model.

Where k_n is the normal spring constant and C_n is the damping coefficient, the normal force is given by

$$F_n = \frac{4}{3} Y \sqrt{R\delta_n^3} \tag{10}$$

where Y is the equivalent Young's Modulus, R is the equivalent radius, and δ is the normal overlap.

The normal damping force is given by

$$F_n^d = -2\sqrt{\frac{5}{6}}\beta\sqrt{S_n m}V_n^{\text{rel}} \tag{11}$$

where m is the equivalent mass, V_n^{rel} is the normal component of the relative velocity, e is the coefficient of restitution, and S_n and β are the normal stiffnesses.

$$S_n = 2Y\sqrt{R\delta_n} \tag{12}$$

$$\beta = \frac{\ln^e}{\sqrt{\ln^e \varepsilon + \pi^2}}$$

Tangential force and tangential overlap are given by

$$F_t = -S_t\delta_t \tag{13}$$

$$F_t^d = -2\sqrt{\frac{5}{6}}\beta\sqrt{S_t m}V_t^{\text{rel}} \tag{14}$$

where the tangential stiffness (S_t) is $S_t = 8G\sqrt{R\delta_n}$, G is the equivalent shear modulus, and V_t^{rel} is the equivalent tangential velocity.

The rolling friction was brought into account by applying a torque to the contacting surfaces

$$\tau_i = -\mu_r F_n R_i \omega_i \tag{15}$$

where μ_r is the coefficient of rolling friction, R_i is the distance of the contact point from the center of mass of the object, and ω_i is the unit angular velocity of the object at the contact point.

Electrostatic force

For charged particles, a long distance force had to be considered according to Coulomb's law. Indeed, the electrostatic potential U of a particle j with a charge q_j on a particle i with a charge q_i induces the following force:

$$\vec{F} = -\frac{\mathrm{d}U}{\mathrm{d}r}\bar{n} \tag{16}$$

in which r is the distance between the center of i and j. The screened Coulomb potential U of particle j decreases exponentially with Debye length λ

$$U = \frac{q_i q_j}{4\pi\varepsilon_0 r}\exp\left(-\frac{r}{\lambda}\right) \tag{17}$$

in which Debye length λ is a function of the charged particles $p_1, p_2, \ldots$ with respective charges $q_{p1}, q_{p2}, \ldots$ in the vicinity of particle j

$$\lambda = \sqrt{\frac{\varepsilon\varepsilon_0 K_B T}{q_e^2 \sum_k q_{pk}^2}} \tag{18}$$

in which ε is the relative permittivity of the medium surrounding the particles, ε_0 is the permittivity of free space, K_B is the Boltzmann's constant, T is the temperature, and $q_e = 1.6 \times 10^{-19} C$ is the charge of an electron. To reduce the simulation runtime, particles further than a specific distance from j are neglected in the calculation of λ (Houge et al., 2008).

In **Figure 11**, particle transportation by electrostatic and electromagnetic forces is shown at different times. At $t = 0.05$ s, particles are lying along the cylinder and there is no electric or magnetic field. At $t = 0.07$ s, the first coil is activated by a DC current that lasts for 1 s. As shown in **Figure 11b**, particles start to experience the forces and levitate from the surface. As DC current was used for the simulation, the fields behaved uniformly. Thereby, as shown in **Figure 11c**, at $t = 0.37$ s, particles gather around the first coil until the activation of the second coil, which happens at $t = 1$ s. After the second coil is activated, the fields will be distorted and particles will change their location based on the new fields and forces (**Figure 11d**, $t = 1.01$ s). The particles stay around the second coil (**Figure 11e**, $t = 1.15$ s) until the third coil is activated, and then they move towards the exit side of the cylinder (**Figure 11f**, $t = 2.08$ s).

Experimental results

The first experiment was set up as shown in **Figure 12**. The prototype was elevated and supported by a wooden stand. A small amount of the regolith dust simulant CHENOBI, containing approximately 2% iron, was placed in the middle of the aluminum tube. Two receptacles were placed under each opening of the tube to collect the dust coming out. A transparent box was placed over the tube to prevent air currents from affecting the results.

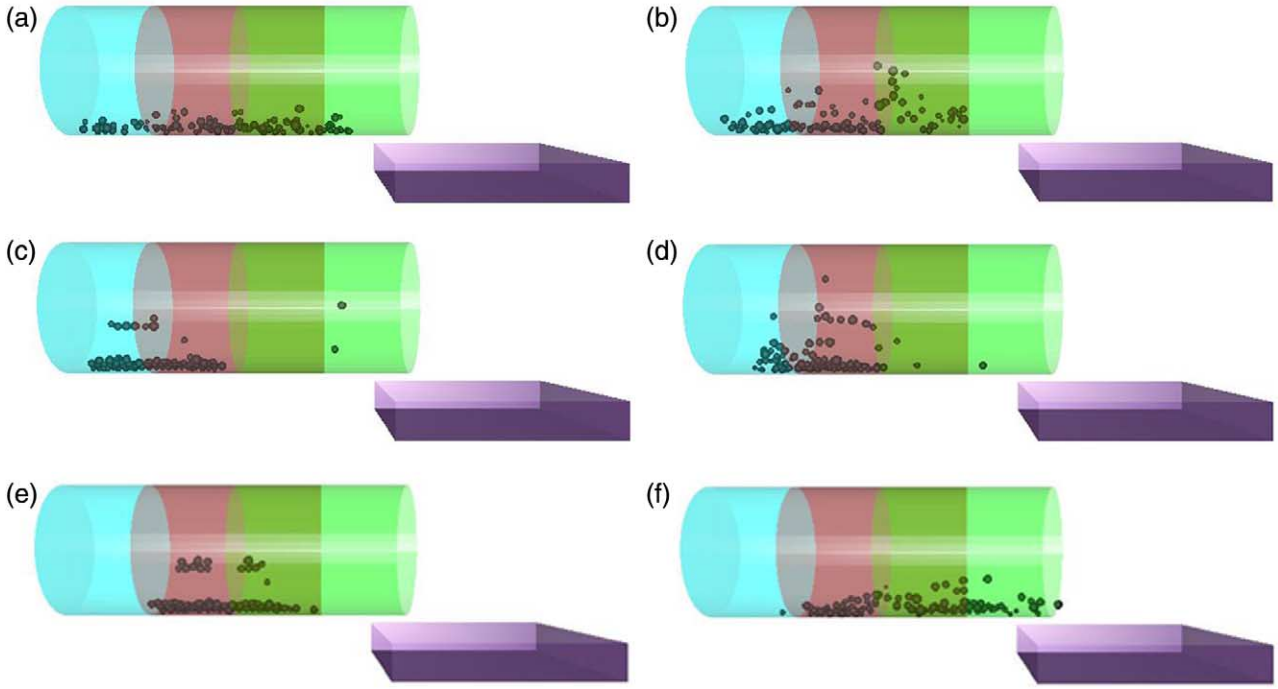

Figure 11. Particle movement at different activation time.

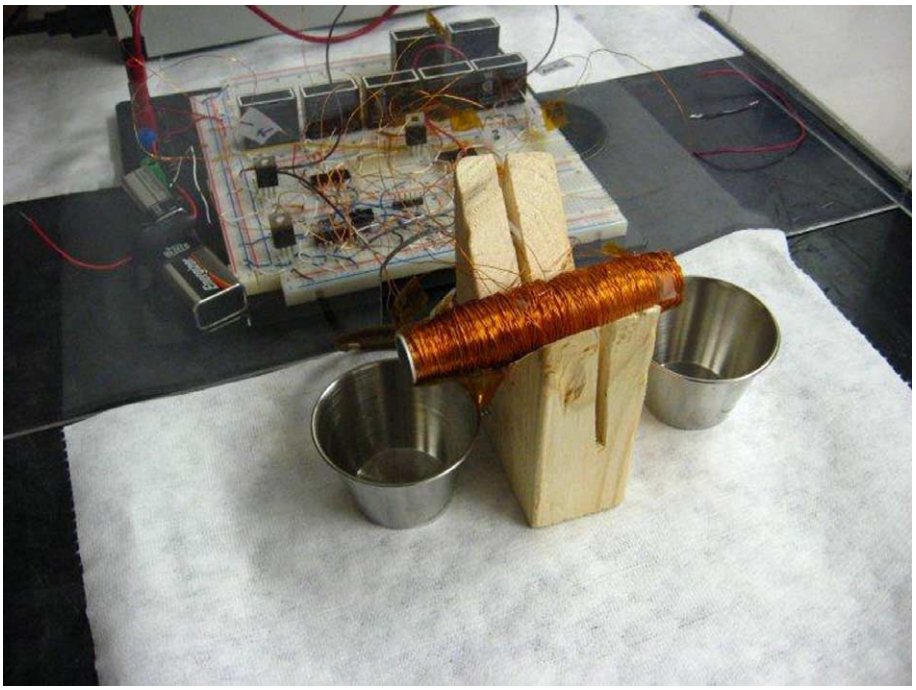

Figure 12. First experimental setup.

The first set-up was made of seven coils that were sequentially activated for a period of 1 s then deactivated. Once the experiment was over, we looked inside the receptacles and observed that the one near coil 7 contained dust. The amount of collected dust was small and the trace it left on a white rag can be seen in the red circle on **Figure 13**.

To obtain better results, a second experiment was conducted. The base of the magnetic peristalsis was the same as the first attempt but the current was provided from capacitors to obtain better burst power values.

The second experiment was set up as shown in **Figure 14**. A shorter version of the power outlet prototype with only

Vol. 59, No. 2, August/août 2013

three coils was designed to simplify the experiment. This second prototype was fitted in a Plexiglas wall. A small amount of the same regolith dust simulant was placed in the middle of coil 1 and a paper towel was placed under the opening of the tube to collect the ejected dust.

As shown in **Figure 15**, regolith simulant was moved towards the opening during the sequential activation of the solenoids. Though most of the dust remained in the tube, some of the stimulant was ejected and collected on the paper towel as shown in **Figure 16**.

Although the dust was not fully expelled, the design will be more effective with real lunar conditions. The lower gravity and the vacuum environment of the moon will diminish the friction of the system. The real lunar regolith might also be more ferromagnetic than the stimulant used in this experiment, thus, more sensitive to the effect of the magnetic peristalsis.

Figure 15. Displacement of regolith simulant.

Figure 13. Collected dust out of coil 7 on a white rag.

Figure 16. Collected dust on a paper towel.

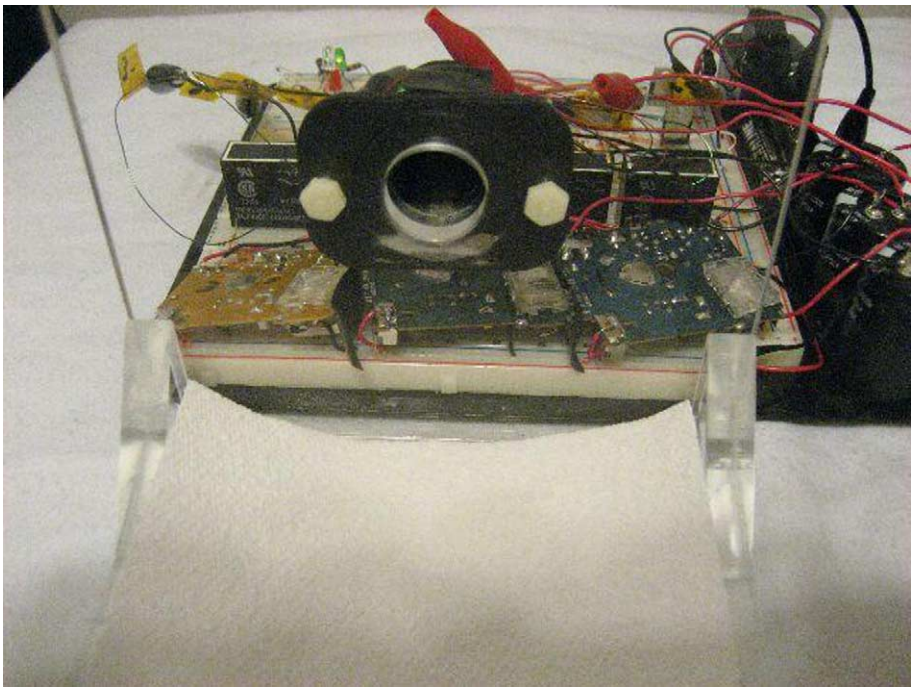

Figure 14. Second experimental setup.

Conclusion

The pervasiveness of lunar dust, as well as its abrasiveness, will complicate any connection tasks on the moon. These connection tasks could be necessary for robotic operations where payloads on the rover could be interchanged. By using a biological phenomenon as inspiration, a design was developed to allow cleaning of the interface before connection. The prototype demonstrated the functionality of the design. The next steps involve constructing a more representative prototype with full connecting ability.

Three sets of coils were simulated to study the effect of electrostatic and electromagnetic fields on particle movements. Both fields were determined using finite element modeling. The resulting fields were then imported in a discrete element modeling software. Smooth particle transportation was observed in the simulation. It was also observed that to optimize the experimental setup, strong enough electric and magnetic fields must be provided to lift the particle from the surface or to overcome the frictional forces between the particles themselves and between the particles and the surface holding the particles. Applying an AC power source rather than a DC power source also improved the efficiency of the device in cleaning the surface from the dust particles. Future studies should focus on the effect of different voltage profiles, frequency, distance between coils, and different types of media.

References

Chiu, I., and Shu, L.H. 2007. Biomimetic Design through Natural Language Analysis to Facilitate Cross-Domain Information Retrieval. *Artificial Intelligence for Engineering Design, Analysis and Manufacturing*, Vol. 21, No. 1, pp. 45–59.

Houge, M.D. et al. 2008. Calculating the trajectories of triboelectrically charged particles using Discrete Element Modeling (DEM). *Journal of Electrostatics*, Vol. 66, pp. 32–38. doi: 10.1016/j.elstat.2007.08.007.

Stubbs, T.J., Vondrak, R.R., and Farrell, W.M. 2005. Impact of Dust on Lunar Exploration, Proceedings of Dust in Planetary System.

Vakili, V., and Shu, L. 2001. Towards Biomimetic Concept Generation, in Proceedings of the 2001 ASME Design Technical Conferences, Design Theory and Methodology Conference, Pittsburgh, PA, U.S.A., September 9–12, 2001, Paper no. DETC2001/DTM-21715.

Zakrajsek, J., McKissock, D., Woytach, J., Zakrajsek, J., Oswald, F., McEntire, K., Hill, G., Abel, P., Eichenberg, D., and Goodnight, T. 2005. Exploration Rover Concepts and Development Challenges, Proc. of 1st AIAA Space Exploration Conference, Orlando, FL, AIAA-2005-2525.